Photochemistry and Photobiology, 2015, 91: 1315–1323

Preparation of Silver Carbonate and its Application as Visible Light-driven Photocatalyst Without Sacrificial Reagent

Wei Jiang*, Ya Zeng, Xiaoyan Wang, Xiaoning Yue, Shaojun Yuan, Houfang Lu and Bin Liang

Multi-phase Mass Transfer and Reaction Engineering Laboratory, College of Chemical Engineering, Sichuan University, Chengdu, China

Received 7 April 2015, accepted 27 June 2015, DOI: 10.1111/php.12495

ABSTRACT

Visible light-driven photocatalyst is the current research focus and silver oxyacid salts with *p*-block elements are the promising candidates. In this research, Ag_2CO_3 was prepared by a facile precipitation method and used to degrade the pollutants from waters. The results revealed that the silver carbonate with monoclinic structure quickly decomposed methyl orange and rhodamine B in less than 15 min under visible light irradiation. When it was recycled six times, the degradation of methyl orange still can reach 87% after 30 min. The calculated band gap of Ag_2CO_3 was 2.312 eV with Valence band edge potential of 2.685 eV and Conduction band 0.373 eV *vs* NHE, which endowed the excellent photooxidation ability of silver carbonate. Photogenerated holes and ozone anion radicals were the primary active species in the photo-oxidization degradation of dye. The generation of metallic silver resulted from photocorrosion and the consequent reduction in the ozone anion radical amount led to the performance degradation of Ag_2CO_3. The simple preparation method and high photocatalytic performance of Ag_2CO_3 increases its prospect of application in future.

INTRODUCTION

Recently, with the development in the field of photocatalysis, the new photocatalysts driven by visible light have attracted more and more attention for production of clean energy and remediation of environmental pollution due to the high solar light utilization rate (1,2). Generally, two main strategies are employed to achieve the visible light-driven photocatalyst: modification of UV light-driven photocatalyst, especially TiO_2 with N (3–5), C (6–8), S (9–11), P (12) and F (13), and design of novel semiconductor materials with narrower band gap energy, such as CdS (14), ZnS (15) and $BiVO_4$(16,17). Among them, the semiconductors containing silver are focused specially owing to their interesting and high-efficient photocatalytic performance. The typical examples include Ag_2O (18) and its derivative Ag-based oxides with *p*-block elements such as $AgVO_3$ (19–22), $AgSbO_3$ (23–25), $AgGaO_2$ (26–28), Ag_3AsO_4 (29) and $AgAlO_2$ (30), which were reported to decompose persistent organic pollutants such as phenol, methylene blue (MB), rhodamine B (RhB), methyl orange (MO) under visible light with eye-catching reaction rate. Especially, Ag_3PO_4 (31–35) exhibited an outstanding photocatalytic performance in photodegradation process of dye, attracting the attentions because of the adding of nonmetallic *p*-block elements. Such noticeable photocatalytic capacity was attributed to the higher valence band and narrower band gap caused by the hybrid of Ag^{4d} orbitals with the O^{2p} orbitals (36). Introducing unoccupied *s*, *p* states of *p*-block elements can effectively tune the potentials of conduction band of the Ag-based oxides. This advisable strategy to achieve better Ag-based photocatalyst to degrade persistent pollutants inspired more attempt by adding different *p*-block elements into Ag-based oxides.

Carbon element is a nonmetallic *p*-block element. Ag_2CO_3 synthesized by Xu *et al.* (37) was used to photodegrade methylene blue and phenol under visible light irradiation. The photodegradation time was more than 40 and 120 min, respectively. The Ag_2CO_3 prepared by this method possessed lower decomposition rate and accompanied with serious performance degradation, and Na_2CO_3 was used as an anticorrosion reagent to retard such undesired performance loss. Another approach was adding $AgNO_3$ to inhibit the photocorrosion effect of Ag_2CO_3, which was attempted by Dai *et al.* (38). However, the performance and stability of Ag_2CO_3 were not satisfactory yet, and the employment of $AgNO_3$ as sacrificial reagent increased the cost, and introduced the new pollution.

In this research, Ag_2CO_3 was prepared by a facile ion-exchange method, and used as visible light-driven photocatalyst to decompose MO and RhB without any additives under Xenon lamp and solar light. The effect of different carbonate precursors on the performance of Ag_2CO_3 was investigated and the stability of as-prepared Ag_2CO_3 samples was studied.

MATERIALS AND METHODS

Materials. Silver nitrate, sodium carbonate, methyl orange (MO), methanol, rhodamine B (RhB) and indigo carmine, all were purchased from Chengdu Kelong Chemical Reagent Company (Chengdu, China), and were used directly as received. Deionized water was used throughout this study.

Preparation of Ag_2CO_3. Ag_2CO_3 nanoparticles were synthesized by a simple ion-exchange precipitation reaction between $AgNO_3$ (0.2 M) and Na_2CO_3 (0.1 M) in liquid phase at room temperature. In a typical procedure, under magnetically stirring, 25 mL of $AgNO_3$ (0.2 M) was added into a 100 mL homemade light-tight beaker, which was encapsulated with tinfoil paper to block light. Subsequently, 55 mL of carbonate (0.1 M) was dropped into the $AgNO_3$ solution by (ZDJ-3D) automatic titrator with dropping speed of 3.2 mL min^{-1}. After dropping finished, keep stirring more than 2.5 h. The admixture was filtered and washed with DI water to remove the unreacted components and by-products.

---

*Corresponding author email: weijiang@scu.edu.cn (Wei Jiang)

Finally, the yellowish powders were vacuum-dried at 40°C for 24 h. All the above steps were conducted in darkroom with red dark room lamp.

Sample characterization. The morphology of the specimens was detected by a JSM-7500F field emission scanning electron microscopy (FESEM, Japan). The structural features were determined using glancing angle X-ray diffraction (GA-XRD, X'Pert proMPD, the Netherlands) with a Cu Kα radiation (wavelength $\lambda = 0.15406$ nm). UV−Vis spectrophotometer (TU-1901, Ge Beijing spectrometer, China) with barium sulfate as the reference was used to acquire the UV−Vis diffusion reflection spectra of Ag_2CO_3 specimens. Fourier transform infrared spectroscopy (FT-IR) of sample was determined with a NEXUS 670. A VG ESCALAB MKII XPS system with Al Kα source and a charge neutralizer was employed to conduct the X-ray photoelectron spectroscopy (XPS) measurements. The specific surface area of samples was determined by a laser particle sizer (JL-6000, Chengdu Jinxin Powder Analyse Instrument Co., Ltd.). An FLsp920 instantaneous spectrometer was utilized to carry out the photoluminescence spectrum (PL) analysis of Ag_2CO_3. The active species in the photocatalytic process of Ag_2CO_3 was probed by electron spin resonance (ESR) with an ER200-SRC.

Evaluation of photocatalytic activity. The photocatalytic activity of the as-prepared samples for decolorization of MO and RhB aqueous solution was examined at ambient temperature in an OCRS-IV photoreactor system with a 500 W Xenon lamp and a UV cut-off filter (Ultraviolet ZJB380 glass, $\lambda > 380$ nm) as the visible light source. The typical detailed experimental procedure is conducted as following: Four 10 mL test tubes filled with 10 mL MO (16 mg L^{-1}) or RhB (16 mg L^{-1}) aqueous solution were used to conduct the parallel testing in dark. Ag_2CO_3 powder (0.1000 g) was dispersed into each tube. The dye solution mixed with Ag_2CO_3 powder was placed in the dark with stirring for 30 min to reach the adsorption equilibrium. The lights were then turned on. At each given time interval, 5 mL suspension was sampled from each tube and centrifuged to remove the Ag_2CO_3 powder. The concentration of MO or RhB during the degradation was monitored via colorimetry by using an UV−Vis spectrophotometer (TU-1810, Beijing). At last the results of four tubes were averaged to determine the decomposition rate of the dye.

In order to research the possibility of applying Ag_2CO_3 for actual system, the photocatalytic performance of Ag_2CO_3 under solar light was carried out according to the above procedure except that the artificial light resource for irradiation was replaced by the natural sunlight in different weather conditions.

DFT simulation conditions. Electronic structure of Ag_2CO_3 was analyzed by the plane wave pseudopotential approach based on the density functional theory (DFT). After geometry optimization, the electronic structure was calculated by using CASTEP code. The GGA was used to describe the exchange and correlation energy of the electrons. The ultrasoft pseudopotential in the Vanderbilt form was used for the ion–electron interaction. The corresponding valence atomic configurations of O, C and Ag were $2s^22p^4$, $2s^22p^2$ and $4d^{10}5s^1$, respectively. The set value of energy cutoff for a plane wave basis was 400 eV, and a 6 × 6×6 Monkhorst-Pack k-mesh is used. The other parameters employed in calculation were as following: 1×10^{-6} eV/atom of the self-consistent convergence accuracy; 0.01 eV of the convergence criterion for the maximal force between atoms; 5×10^{-4} Å of the maximum displacement; 0.02 GPa of the stress; 1×10^{6} eV/atom of the SCF tolerance; 5 eV of the U_p parameter for O and C and 10.2 eV of the U_d parameter for Ag. The Fermi level was as the zero of energy. In addition, only the spin-up results were shown in this paper because of the complete symmetry between spin-up and spin-down states.

RESULTS

The characteristics of the as-prepared Ag_2CO_3 samples

Appearance and morphology. As-prepared yellow fine powders possess a smooth trapezoid single crystal without obvious fracture and an average diameter of 1.5 μm as is shown in Fig. 1A, B. The main particle size distribution ranged from 0.8 to 2 μm (See Supporting Information Fig. S1). Moreover, measured specific surface area of Ag_2CO_3 was about 0.437 $m^2\ g^{-1}$.

Crystal structure. X-ray diffraction (XRD) results in Fig. 1C confirmed that all the diffraction peaks of the as-prepared samples were in good agreement with those of the monoclinic structure of Ag_2CO_3 (No. 26-0339), with space group of P21/m, $a = 4.852(4)$ Å, $b = 9.553(8)$ Å, $c = 9.553(8)$ Å and $\beta = 91.96°$ (39). No peak belonging to metallic silver was observed. However, XPS measurements results shown in Fig. 1D revealed that as-prepared sample was a mixture of 36% metallic Ag and 64% monovalent silver ion. XPS and XRD results suggested that the sample is the hybrid of Ag_2CO_3 and Ag. Such structure could be expected to improve the performance and stability of silver salts under light irradiation due to the plasmon resonance (40–42).

UV–Vis DRS. The ultraviolet–visible diffuse reflectance spectrum (UV–Vis DRS) in Fig. 1E indicated that the yellowish Ag_2CO_3 could absorb solar energy with a wavelength shorter than 480 nm, and the band gap energy estimated from the intercept of the tangent to the plot is 2.30 eV. It should be noticed that the visible edge is steep, sufficiently indicating that the transition from valence band to conduction band is the intrinsic absorption band of Ag_2CO_3, rather than from the impurity to the conduction band.

Further simulation with DFT in Fig. 1F confirmed that the indirect band gap and direct band gap of Ag_2CO_3 was 2.312 eV and 2.812 eV, respectively. The indirect band gap and the direct band gap at the Q point are energetically close, and steep rise occurs in photocurrent. The corresponding partial DOS (PDOS) presented in Supporting Information Fig. S2 confirmed that the root of the main difference of the valence band (VB) should ascribe to the difference of the Ag 4d PDOS calculated by $U_{d,Ag} = 7.2$ eV and $U_{d,Ag} = 10.2$ eV. Due to the small band gap, Ag_2CO_3 should harvest visible light. The value of valence band and conduction band of Ag_2CO_3 can be obtained based on the experimental value of band gap and the following equation (40):

$$E_{VB} = X - E_e + 0.5E_g,$$

where E_{VB}, E_e and E_g are the valence band, free electron energy on the hydrogen scale (ca. 4.5 eV) and the band gap of Ag_2CO_3, respectively. X is the calculated Pearson absolute electronegativity of the Ag_2CO_3.

The calculated value of valence band E_{VB} of Ag_2CO_3 was 2.685 eV, and consequently the bottom of conduction band E_{CB} was 0.373 eV *vs* NHE.

Photodegradation of MO and RhB with Ag_2CO_3 and its stability

Photodegradation of two typical organic dyes, methyl orange (MO) and rhodamine B (RhB), were conducted to exhibit the photo-oxidative ability of Ag_2CO_3, without any additives as electron acceptor. The corresponding standard absorption curves of MO and RhB solution are shown in Supporting Information Fig. S3.

The adsorption of two dyes on the Ag_2CO_3 powder was taken into account and determined, which only 5% initial concentration of MO, and 9% of RhB was adsorbed when equilibrium was reached in the dark after half an hour with sufficient stirring (See Supporting Information Fig. S4). The pH value of the solution was kept at the value of deionized water during the reaction. In order to exclude the interference of the self photodegradation effect of dye under visible light irradiation, photodegradation of MO and RhB under the same conditions without photocatalyst was carried out (See Supporting Information Fig. S5), and the

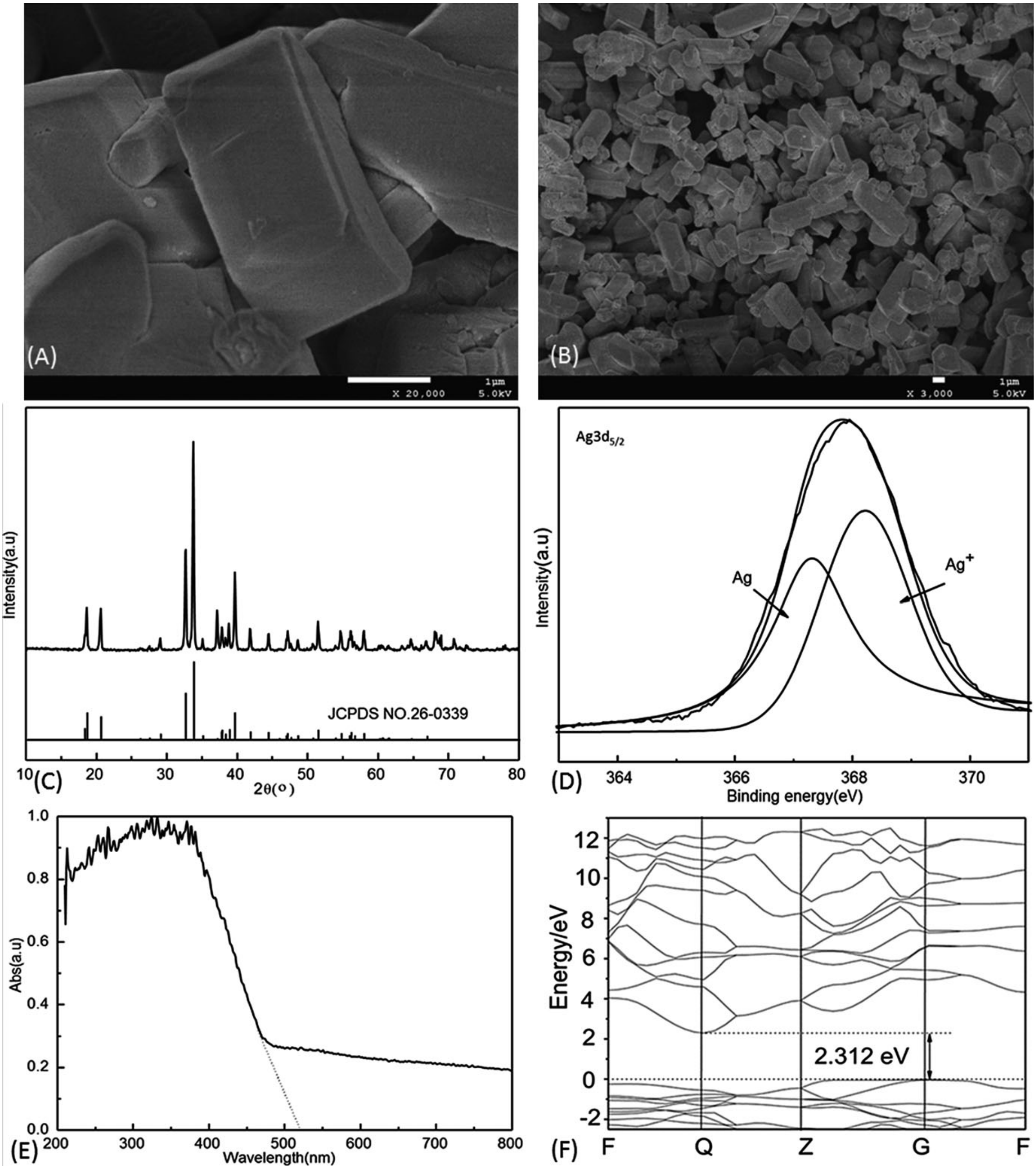

Figure 1. The characterization of as-prepared fresh Ag_2CO_3: (A) SEM × 3000; (B) SEM × 20 000; (C) XRD pattern; (D) XPS results of Ag $3d_{5/2}$ peak; (E) UV–Vis DRS from 200 nm to 800 nm; (F) Energy-band diagram of Ag_2CO_3 calculated by a density functional method.

results showed that the self photodegradation of dye can be negligible.

Figure 2 showed the fast decreasing tendency of MO and RhB against light illumination time over Ag_2CO_3. The profile displayed the high photo-oxidation activity of Ag_2CO_3. When the Ag_2CO_3 was used at the first time, the degradation of MO could reach 98% after 14 min. After Ag_2CO_3 was recycled six times, the degradation of MO can also reach 87% after 30 min in Fig. 2A. Furthermore, the performances and stability of Ag_2CO_3 in photodegradation of RhB was in accordance with the

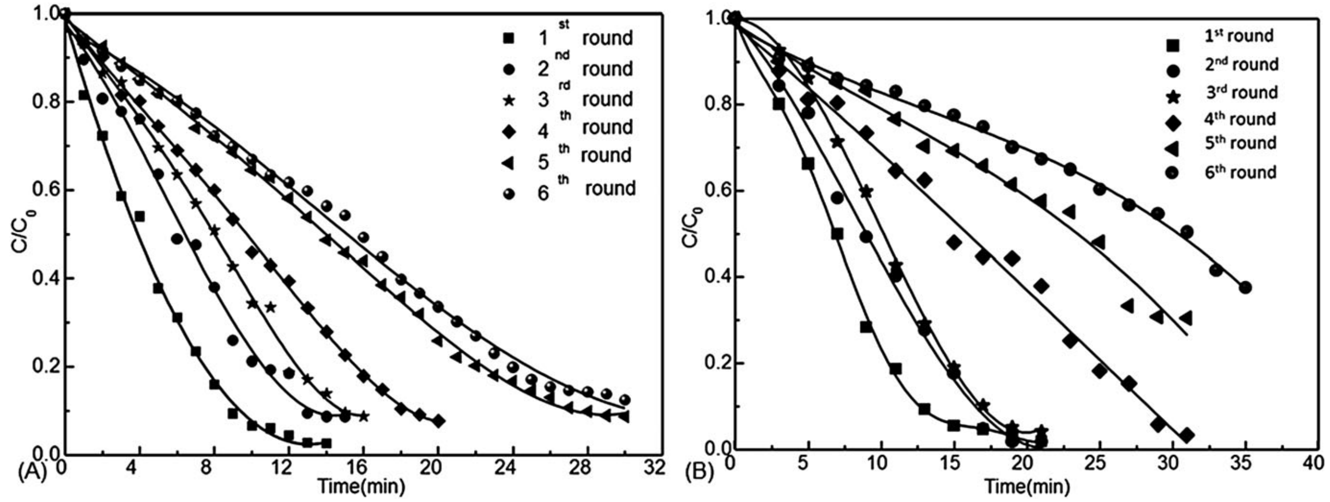

Figure 2. The photoactivity and stability of Ag_2CO_3 by degradation of (A) MO and (B) RhB.

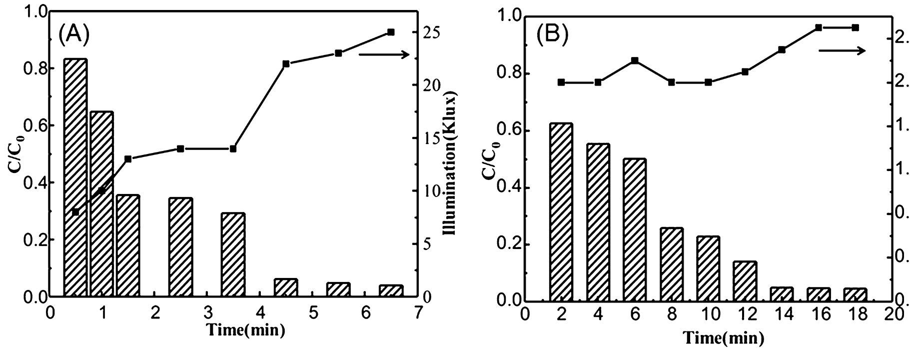

Figure 3. Degradation of MO with Ag_2CO_3 under solar light irradiation: (A) sunny day; (B) cloudy day.

MO in Fig. 2B. The degradation of RhB was about 98% first and 62% after Ag_2CO_3 was recycled six times. When the Ag_2CO_3 was used at the first time, the full UV–Vis absorption spectra of MO and RhB solution in photocatalytic degradation process against time were shown in Supporting Information Fig. S6. The corresponding time consumed increased from 14 to 32 min because of recycling. Other researchers' results, by contrast, spent more than 18 min to degrade 90% RhB (38), which used a simple facile precipitation reaction between $NaHCO_3$ and $AgNO_3$. Obviously, the performance and stability of the silver carbonate were better than that reported in literature (37,38). The oxidative performance and stability of self-made Ag_3PO_4 was tested under the same conditions and provided as a comparison (See Supporting Information Fig. S7). It can be found that the photocatalytic performance of Ag_2CO_3 is roughly equivalent to Ag_3PO_4 when used at the first time; however, the performance stability of the former is significantly better than the latter. It is worth noting that the excellent performance of Ag_2CO_3 was achieved without adding any sacrificial reagents.

Herein, in order to investigate the possibility of applying Ag_2CO_3 for actual system (43), the experiments of photodegradation of MO with Ag_2CO_3 under solar light in sunny or cloudy day was proceeded, and the results were demonstrated in Fig. 3A,B, respectively. The dye was decomposed completely in 4.5 min in sunny day with average light illumination of 22 Klux, and in 14 min in cloudy day with 2.3 Klux. Apparently, the relative slow degradation of MO in cloudy day should ascribe to the relatively weak light irradiation.

Characterization of used catalyst

The photocatalytic performance of used Ag_2CO_3 could be investigated with SEM, XPS and XRD analysis. SEM picture of Ag_2CO_3 catalyst after six cycles in Fig. 4A,B exhibited the unsmooth outward appearance with many fissures and holes on the surface of crystal, which can be regarded as the consequence of photocorrosion. The XPS result in Fig. 4C clearly showed that the shoulder peak of metallic Ag at 367.9 eV was enlarged comparing with the Ag^+ peak at 367.6 eV after six cycle, and the calculated ratio of metallic Ag to monovalent silver ion increased to 58.3:41.7, which suggested that it was the generation of metallic silver that resulted in the performance degradation of Ag_2CO_3. The peak of generated Ag simple substance was also easily observed in the results of XRD in Fig. 4D. Such tendency meant that the stability of Ag_2CO_3 depended significantly on the decomposing rate of salts to metallic silver. However, this performance decaying rate of Ag_2CO_3 after repeated using was slower than that of Ag_3PO_4 since its ratio of Ag to Ag+ increased from 37.7:62.3 to 77.5:22.5 after reusing. The detailed comparison was shown in Supporting Information Fig. S8. It could be summarized that the stability of Ag_2CO_3 under light irradiation was relatively excellent.

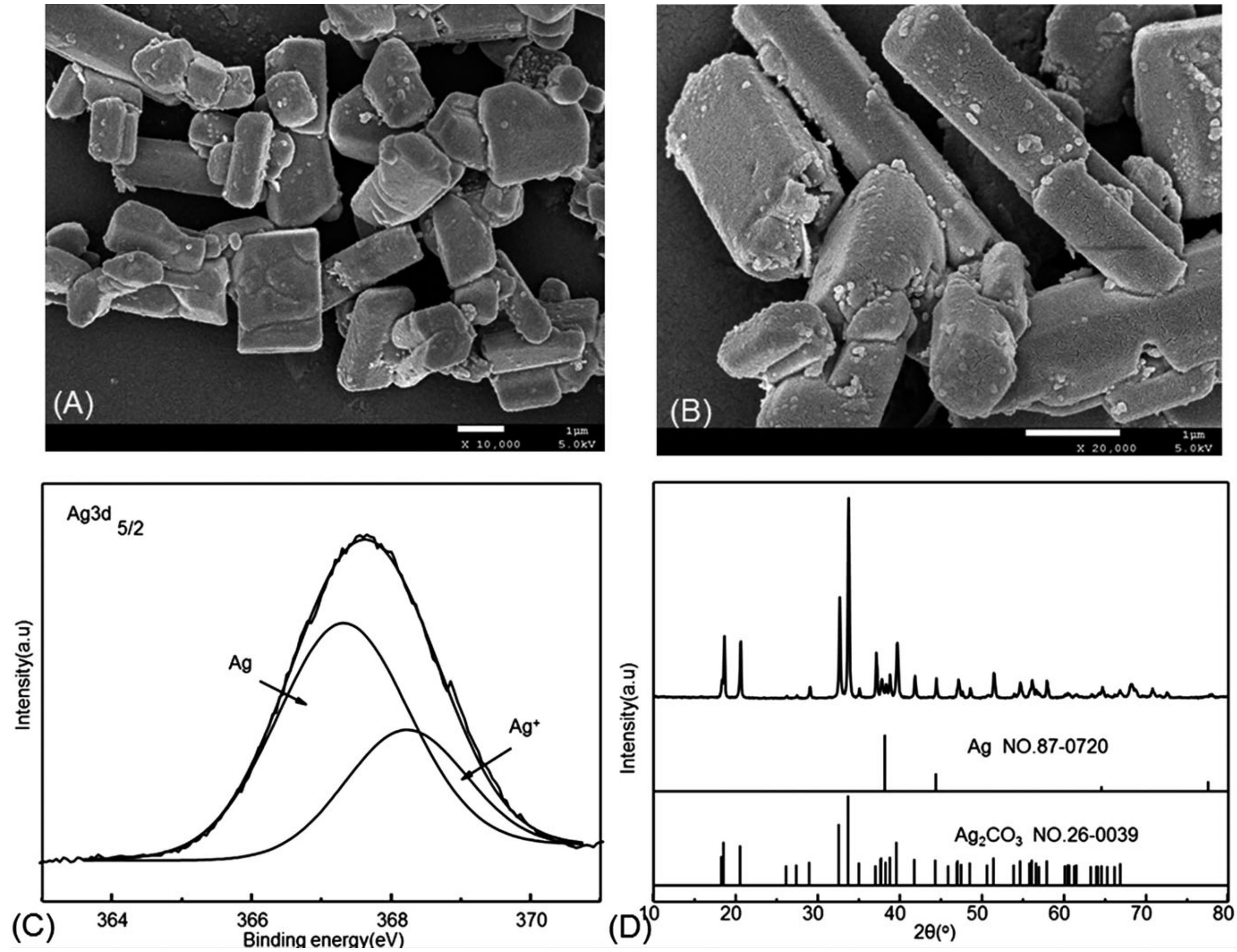

Figure 4. The characterization of used Ag_2CO_3 after six cycles: (A) SEM × 10 000; (B) SEM × 20 000; (C) XPS results of Ag $3d_{5/2}$ peak; (D) XRD pattern.

Photodegradation mechanism of Ag_2CO_3

Generally three possible active species were considered in a typical photodegradation mechanism analysis: photogenerated holes, hydroxyl radicals and superoxide anion radicals. In this research, it is reasonable to exclude the possibility of the two latters participating in the photodegradation reaction because the electrode potential of $\bullet OH$ radicals is 2.80 eV, and $\bullet O_2^-$ radicals is -0.046 eV, which is beyond the calculated redox potential range of Ag_2CO_3 under visible light irradiation. The photogenerated hole of Ag_2CO_3 is the latent active specie, but the other possible candidates cannot be eliminated directly since multiple oxygen-derived free radicals could be generated in a photochemical process. Thus, ESR analysis and radical-trapping experiment (44) were carried out to determine the possible active species, constructing the photodegradation mechanism of Ag_2CO_3.

ESR analysis. The ESR analysis results of fresh and used Ag_2CO_3 in dark and with light at different time were shown in Fig. 5. The plots confirmed that only ozone anion radicals, $\bullet O_3^-$ were observed since the seven line spectrums have been detected (42,45,46). Furthermore, no any signals judged as superoxide anion radicals or hydroxyl radical ware observed. At starting time, 0 min, almost no observable peaks were found, but with the lighting time expansion, the ESR signal of ozone anion radicals increased sharply, which confirmed that such signal was induced by the light. After light irradiation, the seven line spectrums signal intensity was significantly strengthened. Therefore, the ozone anion radicals can be considered as the probable active specie in the photocatalytic process of Ag_2CO_3.

It is worth mentioning that the signal strength of fresh Ag_2CO_3 is higher than that of reused sample after light irradiation. Such result confirms the conclusion surmised from results of XRD and XPS, and is a complement to the deduction that performance degradation of Ag_2CO_3 is because of the decreasing of the $\bullet O_3^-$ radicals amount resulted by the decrease of Ag^+ ion amount. As the electrode potential of ozone in neutral solution is 1.24 eV, the ozone should generate from the dissolved oxygen in solution after light irradiation, and obtain the photogenerated electron to form ozone anion radical. At same time, because the CB potential of Ag_2CO_3 is lower than the electrode potential of $Ag/AgNO_3$ (0.80 eV), Ag^+ ion should also attract the photogen-

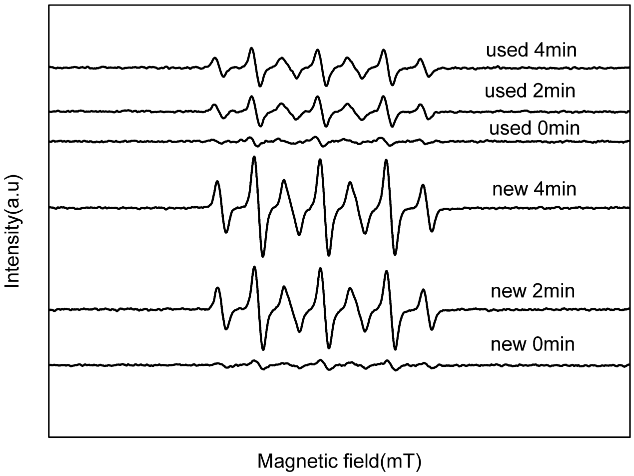

Figure 5. ESR signals of Ag_2CO_3 without light irradiation and with light irradiation.

erated electron to be reduced to metallic Ag. Besides, it is worth noted that the performance degradation tendency of Ag_2CO_3 also weakens, which indicates that the reduction of Ag^+ ion and the generation of $\bullet O_3^-$ are competitive under visible light irradiation. This is one of the reasons why Ag_2CO_3 is efficient in degradation of organic pollutant.

Radical-trapping experiments. For further determining the existence of $^{\bullet}O_3^-$ radicals and investigating its function in photodegradation process of Ag_2CO_3, a radical-trapping experiment was conducted, and indigo carmine and methanol were used as trapping agent for generated ozone and hole, respectively. The possible masking effect of the scavengers for MO detection in spectrophotometry analysis was excluded based on the results in Supporting Information Fig. S9.

The results shown in Fig. 6A confirmed that the respective addition of methanol or indigo carmine retarded the photocatalytic activity of Ag_2CO_3 significantly. The simultaneous adding of two trapping agents terminated the MO photodegradation process with Ag_2CO_3 as photocatalyst under visible light irradiation. Same termination effect of photoreaction was observed in photodegradation process of RhB with Ag_2CO_3, which was shown in Fig. 6B.

The indigo carmine solution with different concentration was used to determine the ozone generation rate of Ag_2CO_3 in solution under visible light irradiation. The results in Fig. 7 confirmed that ozone was generated continuously with silver carbonate under light illumination. The generation speed of ozone almost kept constant, and consequently, the eliminating speed of indigo carmine was proportional to the initial concentration of dye. The calculated generation speed of ozone radicals was 0.034 mmol per catalyst weight (*g*) per minute.

PL analysis. The PL spectra of the Ag_2CO_3 was measured and compared with Ag_3PO_4 in Fig. 8. Weaker emission intensity of Ag_2CO_3 than Ag_3PO_4 demonstrated the less recombination rate of photogenerated hole and electron and consequently higher quantum efficiency, which means stronger photo-oxidability. The fact further confirmed the importance of the more separated photogenerated carriers of Ag_2CO_3 in enhancing their photocatalytic activity. This is another important reason for the excellent photocatalytic performance of Ag_2CO_3.

Proposed photocatalytic process mechanism

Considering the above facts, the measured and calculated redox potentials of Ag_2CO_3 and other possible related substances in the photodegradation process were marked in Fig. 9A, and the proposed photoreaction process of dye on the surface of Ag_2CO_3 under visible light irradiation was described in Fig. 9B. After photogenerating under visible light irradiation, the hole and electron pair of Ag_2CO_3 could separate, mineralizing the organic pollutants, or recombine, releasing fluorescent light. The strong photo-oxidative capacity of Ag_2CO_3 under visible light irradiation should originate from its unrecombined holes themselves, and the ozone anion radicals derived from the reaction between transmitted energetic electrons and the dissolved oxygen. Another undesired side reaction was the

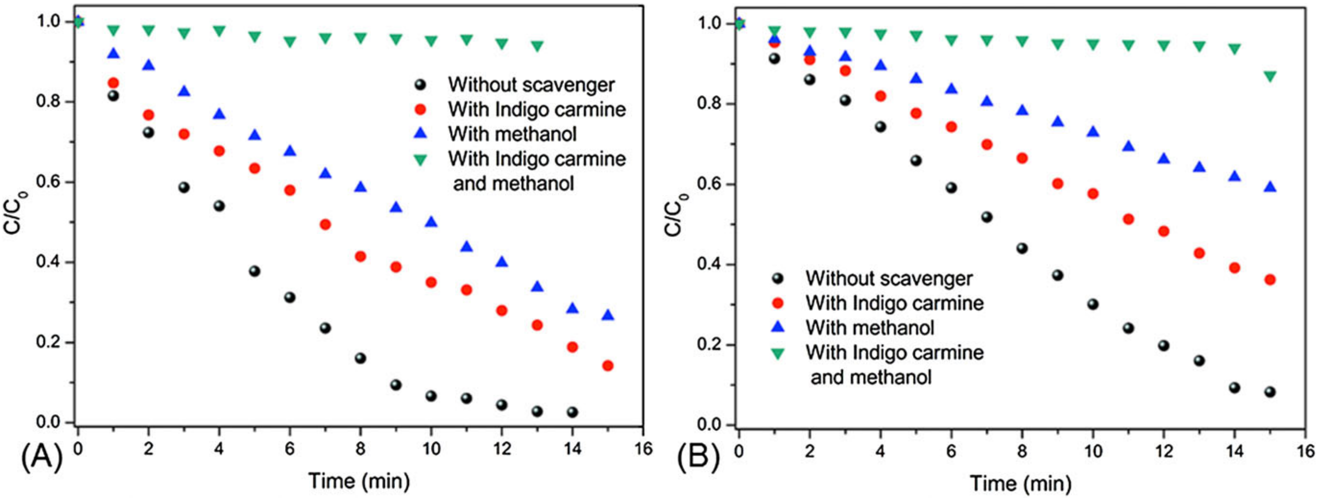

Figure 6. (A) MO and (B) RhB degradation rate with different scavengers by Ag_2CO_3 under light irradiation.

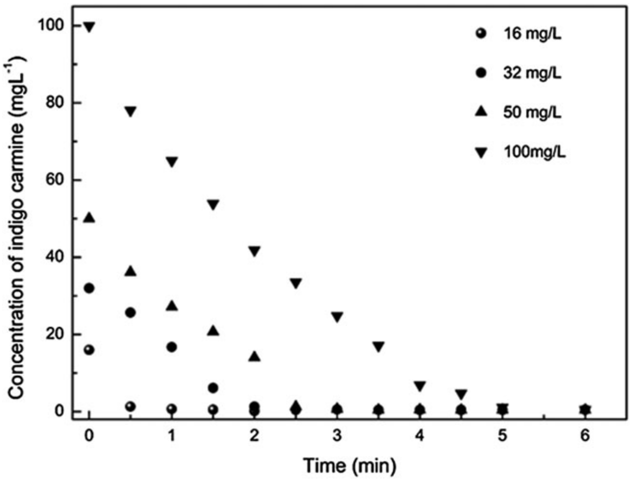

Figure 7. The eliminating speed of indigo carmine with Ag_2CO_3 under visible light illumination.

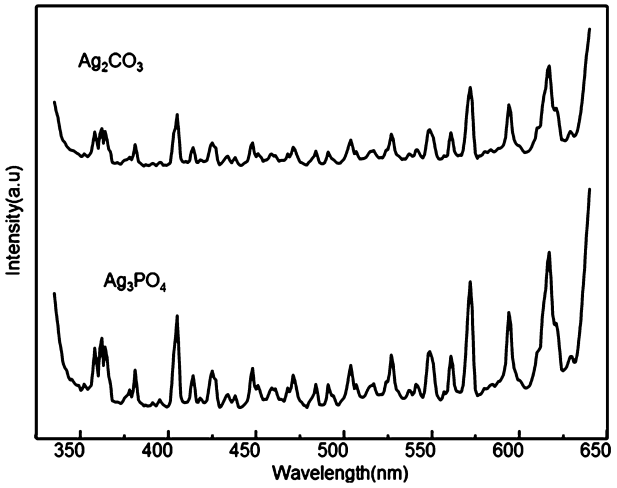

Figure 8. Photoluminescence spectra from 300 nm to 650 nm of as-prepared Ag_2CO_3 sample with Ag_3PO_4 powder as contrast.

reduction of lattice Ag+ with transmitted electron, resulting in the generation of metallic Ag and lowering the photocatalytic performance of Ag_2CO_3.

The photoreactions of Ag_2CO_3 were explained in detail as the following steps:

$$Ag_2CO_3 + hv \rightarrow e^- + h^+$$

$$3O_2 \rightarrow 2O_3$$

$$O_3 + e^- \rightarrow {}^\bullet O_3^-$$

$$\text{dye} + h^+ \rightarrow \ldots \rightarrow CO_2 + H_2O$$

$$\text{dye} + {}^\bullet O_3^- \rightarrow \ldots \rightarrow CO_2 + H_2O$$

$$Ag^+ + e^- \rightarrow Ag$$

CONCLUSION

In summary, a novel visible light-responsive photocatalyst, Ag_2CO_3, was successfully prepared by facile precipitation. Its band gap is 2.312 eV, and VB and CB edge potentials were calculated to be 2.685 and 0.373 eV, respectively. Excellent photooxidation performance and stability of as-prepared Ag_2CO_3 without any sacrificial reagents were shown by photodegradation of MO and RhB. When it was used for the first time, 98% of MO was decomposed no more than 15 min, and after recycled six times, the degradation of MO also can reach 87% after 30 min. In addition as-prepared sample is proved to be practical in actual situations. Based on these demonstrations, the performance decreased gradually due to the decomposition of Ag_2CO_3 to form metallic Ag. In the photocatalytic process of Ag_2CO_3, the photogenerated holes and ozone anion radicals were the decisive active species for the degradation of dye. This work not only uses a simple method to synthesize a novel efficient photocatalyst that can be used for degradation of organic pollutants, but also confirms the important role of ozone played in the photo-oxidative process when the band gap of photocatalyst does not cover the electrode potential range of hydroxyl radicals. This interesting theory deepens insight into the mechanism of photocatalytic degradation of organic pollutants with narrow band gap photocatalyst, and provides a possible approach to enhance the performance and stability of photocatalyst in future.

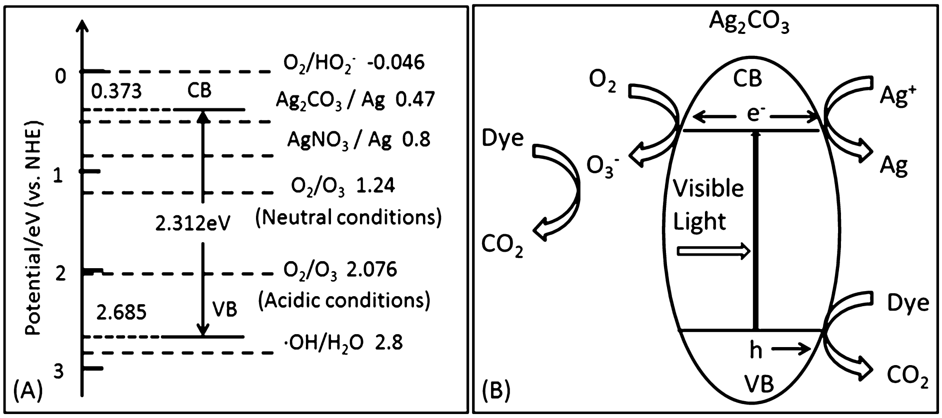

Figure 9. The diagram of photocatalysis mechanism of Ag_2CO_3 under light irradiation: (A) schematic of redox potentials; (B) reaction process.

Acknowledgement—This work was supported financially by the National Natural Science Foundation of China (No. 21176157 and No. 21476146).

SUPPORTING INFORMATION

Additional Supporting Information may be found in the online version of this article:

Figure S1. The particle size distribution of Ag_2CO_3 samples.

Figure S2. Density of states (DOS) simulation of Ag_2CO_3.

Figure S3. Standard curve of MO solution and RhB solution.

Figure S4. The adsorption of MO and RhB on the surface of Ag_2CO_3 without light illumination.

Figure S5. Self-degradation of MO and RhB solution under light irradiation without Ag_2CO_3.

Figure S6. UV–Vis absorption spectra of MO and RhB solution during photodegradation process by Ag_2CO_3 at the first cycle.

Figure S7. The photocatalytic performance comparison of fresh Ag_2CO_3 and Ag_3PO_4; the consuming time for reaching the 90% degradation rate of MO with Ag_2CO_3 and Ag_3PO_4 as photocatalysts in recycling.

Figure S8. XPS results of fresh Ag_3PO_4 and used Ag_3PO_4 sample after six cycles.

Figure S9. The spectrophotometer spectra of solutions of MO with different scavengers

REFERENCES

1. Ni, M., M. K. Leung, D. Y. Leung and K. Sumathy (2007) A review and recent developments in photocatalytic water-splitting using TiO2 for hydrogen production. *Renew. Sust. Energ. Rev.* **11**, 401–425.
2. Chen, C., W. Ma and J. Zhao (2010) Semiconductor-mediated photodegradation of pollutants under visible-light irradiation. *Chem. Soc. Rev.* **39**, 4206–4219.
3. Nakamura, R., T. Tanaka and Y. Nakato (2004) Mechanism for visible light responses in anodic photocurrents at N-doped TiO2 film electrodes. *J. Phys. Chem. B.* **108**, 10617–10620.
4. Jagadale, T. C., S. P. Takale, R. S. Sonawane, H. M. Joshi, S. I. Patil, B. B. Kale and S. B. Ogale (2008) N-doped TiO2 nanoparticle based visible light photocatalyst by modified peroxide sol− gel method. *J. Phys. Chem. C* **112**, 14595–14602.
5. Mrowetz, M., W. Balcerski, A. Colussi and M. R. Hoffmann (2004) Oxidative power of nitrogen-doped TiO2 photocatalysts under visible illumination. *J. Phys. Chem. B.* **108**, 17269–17273.
6. Chen, D., Z. Jiang, J. Geng, Q. Wang and D. Yang (2007) Carbon and nitrogen co-doped TiO2 with enhanced visible-light photocatalytic activity. *Ind. Eng. Chem. Res.* **46**, 2741–2746.
7. Choi, Y., T. Umebayashi and M. Yoshikawa (2004) Fabrication and characterization of C-doped anatase TiO 2 photocatalysts. *J. Mater. Sci.* **39**, 1837–1839.
8. Ren, W., Z. Ai, F. Jia, L. Zhang, X. Fan and Z. Zou (2007) Low temperature preparation and visible light photocatalytic activity of mesoporous carbon-doped crystalline TiO2. *Appl. Catal. B* **69**, 138–144.
9. Chen, X. and C. Burda (2008) The electronic origin of the visible-light absorption properties of C-, N-and S-doped TiO2 nanomaterials. *J. Am. Chem. Soc.* **130**, 5018–5019.
10. Ho, W., J. C. Yu and S. Lee (2006) Low-temperature hydrothermal synthesis of S-doped TiO2 with visible light photocatalytic activity. *J. Solid State Chem.* **179**, 1171–1176.
11. Liu, H. and L. Gao (2004) (Sulfur, Nitrogen)-codoped rutile-titanium dioxide as a visible-light-activated photocatalyst. *J. Am. Ceram. Soc.* **87**, 1582–1584.
12. Iwase, M., K. Yamada, T. Kurisaki, O. O. Prieto-Mahaney, B. Ohtani and H. Wakita (2013) Visible-light photocatalysis with phosphorus-doped titanium (IV) oxide particles prepared using a phosphide compound. *Appl. Catal. B* **132**, 39–44.
13. Jimmy, C. (2006) Synthesis of hierarchical nanoporous F-doped TiO2 spheres with visible light photocatalytic activity. *Chem. Commun.* **10**, 1115–1117.
14. Ran, J., J. Yu and M. Jaroniec (2011) Ni (OH)2 modified CdS nanorods for highly efficient visible-light-driven photocatalytic H2 generation. *Green Chem.* **13**, 2708–2713.
15. Zhang, J., J. Yu, Y. Zhang, Q. Li and J. R. Gong (2011) Visible light photocatalytic H2-production activity of CuS/ZnS porous nanosheets based on photoinduced interfacial charge transfer. *Nano Lett.* **11**, 4774–4779.
16. Li, G., D. Zhang and J. C. Yu (2008) Ordered mesoporous BiVO4 through nanocasting: A superior visible light-driven photocatalyst. *Chem. Mater.* **20**, 3983–3992.
17. Zhang, X., Z. Ai, F. Jia, L. Zhang, X. Fan and Z. Zou (2007) Selective synthesis and visible-light photocatalytic activities of BiVO4 with different crystalline phases. *Mater. Chem. Phys.* **103**, 162–167.
18. Wei, J., X. Y. Wang, Z. M. Wu, X. N. Yue, S. J. Yuan, H. F. Lu and B. Liang (2015) Silver oxide as superb and stable photocatalyst under visible and near-infrared light irradiation and its photocatalytic mechanism. *Ind. Eng. Chem. Res.* **54**, 832–841.
19. Konta, R., H. Kato, H. Kobayashi and A. Kudo (2003) Photophysical properties and photocatalytic activities under visible light irradiation of silver vanadates. *Phys. Chem. Chem. Phys.* **5**, 3061–3065.
20. Hu, X. and C. Hu (2007) Preparation and visible-light photocatalytic activity of Ag3VO4 powders. *J. Solid State Chem.* **180**, 725–732.
21. Huang, C.-M., K.-W. Cheng, G.-T. Pan, W.-S. Chang and T. C.-K. Yang (2010) CTAB-assisted hydrothermal synthesis of silver vanadates and their photocatalytic characterization. *Chem. Eng. Sci.* **65**, 148–152.
22. Pan, G.-T., M.-H. Lai, R.-C. Juang, T.-W. Chung and T. C.-K. Yang (2011) Preparation of visible-light-driven silver vanadates by a microwave-assisted hydrothermal method for the photodegradation of volatile organic vapors. *Ind. Eng. Chem. Res.* **50**, 2807–2814.
23. Shi, J., J. Ye, Q. Li, Z. Zhou, H. Tong, G. Xi and L. Guo (2012) Single-crystal nanosheet-based hierarchical AgSbO3 with exposed 001 facets: Topotactic synthesis and enhanced photocatalytic activity. *Chem.-Eur. J.* **18**, 3157–3162.
24. Singh, J. and S. Uma (2009) Efficient photocatalytic degradation of organic compounds by ilmenite AgSbO3 under visible and UV light irradiation. *J. Phys. Chem. C* **113**, 12483–12488.
25. Kako, T., N. Kikugawa and J. Ye (2008) Photocatalytic activities of AgSbO3 under visible light irradiation. *Catal. Today* **131**, 197–202.
26. Maruyama, Y., H. Irie and K. Hashimoto (2006) Visible light sensitive photocatalyst, delafossite structured α-AgGaO2. *J. Phys. Chem. B.* **110**, 23274–23278.
27. Dong, H., Z. Li, X. Xu, Z. Ding, L. Wu, X. Wang and X. Fu (2009) Visible light-induced photocatalytic activity of delafossite AgMO2 (M= Al, Ga, In) prepared via a hydrothermal method. *Appl. Catal. B* **89**, 551–556.
28. Ouyang, S., N. Kikugawa, D. Chen, Z. Zou and J. Ye (2009) A systematical study on photocatalytic properties of AgMO2 (M= Al, Ga, In): Effects of chemical compositions, crystal structures, and electronic structures. *J. Phys. Chem. C* **113**, 1560–1566.
29. Jianting, T., L. Yong, L. Hai, T. Zhen and L. Datang (2013) A novel Ag3AsO4 visible-light-responsive photocatalyst: Facile synthesis and exceptional photocatalytic performance. *Chem. Commun.* **49**, 5498–5500.
30. Ouyang, S., H. Zhang, D. Li, T. Yu, J. Ye and Z. Zou (2006) Electronic structure and photocatalytic characterization of a novel photocatalyst AgAlO2. *J. Phys. Chem. B.* **110**, 11677–11682.
31. Yi, Z., J. Ye, N. Kikugawa, T. Kako, S. Ouyang, H. Stuart-Williams, H. Yang, J. Cao, W. Luo and Z. Li (2010) An orthophosphate semiconductor with photooxidation properties under visible-light irradiation. *Nat. Mater.* **9**, 559–564.
32. Wang, H., Y. Bai, J. Yang, X. Lang, J. Li and L. Guo (2012) A facile way to rejuvenate Ag3PO4 as a recyclable highly efficient photocatalyst. *Chem.-Eur. J* **18**, 5524–5529.

33. Liang, Q., W. Ma, Y. Shi, Z. Li and X. Yang (2012) Hierarchical Ag 3 PO 4 porous microcubes with enhanced photocatalytic properties synthesized with the assistance of trisodium citrate. *Cryst. Eng. Comm.* **14**, 2966–2973.
34. Bi, Y., H. Hu, S. Ouyang, G. Lu, J. Cao and J. Ye (2012) Photocatalytic and photoelectric properties of cubic Ag3PO4 sub-microcrystals with sharp corners and edges. *Chem. Commun.* **48**, 3748–3750.
35. Dinh, C.-T., T.-D. Nguyen, F. Kleitz and T.-O. Do (2011) Large-scale synthesis of uniform silver orthophosphate colloidal nanocrystals exhibiting high visible light photocatalytic activity. *Chem. Commun.* **47**, 7797–7799.
36. Belver, C., C. Adan and M. Fernández-García (2009) Photocatalytic behaviour of Bi2MO6 polymetalates for rhodamine B degradation. *Catal. Today* **143**, 274–281.
37. Xu, C., Y. Liu, B. Huang, H. Li, X. Qin, X. Zhang and Y. Dai (2011) Preparation, characterization, and photocatalytic properties of silver carbonate. *Appl. Surf. Sci.* **257**, 8732–8736.
38. Dai, G., J. Yu and G. Liu (2012) A new approach for photocorrosion inhibition of Ag2CO3 photocatalyst with highly visible-light-responsive reactivity. *J. Phys. Chem. C* **116**, 15519–15524.
39. Masse, R., J. Guitel and A. Durif (1979) Structure du carbonate d'argent. *Acta Crystallogr. B* **35**, 1428–1429.
40. Wang, P., B. Huang, X. Qin, X. Zhang, Y. Dai, J. Wei and M. H. Whangbo (2008) Ag@ AgCl: A highly efficient and stable photocatalyst active under visible light. *Angew. Chem. Int. Ed.* **47**, 7931–7933.
41. Wang, P., B. Huang, X. Zhang, X. Qin, H. Jin, Y. Dai, Z. Wang, J. Wei, J. Zhan and S. Wang (2009) Highly efficient visible-light plasmonic photocatalyst Ag@ AgBr. *Chem. -Eur. J* **15**, 1821–1824.
42. Smith, W., S. Mao, G. Lu, A. Catlett, J. Chen and Y. Zhao (2010) The effect of Ag nanoparticle loading on the photocatalytic activity of TiO2 nanorod arrays. *Chem. Phys. Lett.* **485**, 171–175.
43. Ye, M., Z. Chen, J. Shen, Y. Ben and X. Liu (2008) ESR analysis on the ozone enhanced photocatalytic activity of aqueous nanosized titanium dioxide suspensions. *Imag. Sci. Photochem.* **26**, 460–467.
44. Kubacka, A., M. Fernández-García and G. Colón (2011) Advanced nanoarchitectures for solar photocatalytic applications. *Chem. Rev.* **112**(3), 1555–1614.
45. Fox, M. A. and M. T. Dulay (1993) Heterogeneous photocatalysis. *Chem. Rev.* **93**, 341–357.
46. Xu, Y. and M. A. Schoonen (2000) The absolute energy positions of conduction and valence bands of selected semiconducting minerals. *Am. Mineral.* **85**, 543–556.